

PACS numbers: 42.62.Eh; 32.80.Pj; 42.50Vk, 32.60.+i
DOI: 10.1070/QE2004v034n12ABEH002749

Use of cold cesium atoms in quantum frequency standards

Yu.S. Domnin, G.A. Elkin, A.V. Novoselov, V.N. Baryshev,
L.N. Kopylov, Yu.M. Malyshev, V.G. Pal'chikov

***Abstract*. The results of studies devoted to the development of a new generation quantum frequency standard, a cesium fountain, are presented. The experimental data obtained upon manipulation and detection of cold atoms are analysed. The cooling of cesium atoms down to about 2 μK is demonstrated experimentally. The populations of hyperfine-structure components of cesium atoms are calculated by the method of adiabatic passage for different microwave pulses.**

Keywords: *cesium frequency standard, laser cooling, optical trapping of atoms, atomic fountain.*

1. Introduction

The time unit – a second in the SI system, is reproduced independently with the help of the State primary time and frequency standard of Russia using the MTsR102 cesium frequency reference [1, 2]. At present, the main metrological characteristic of the MTsR102 reference – a non-excluded systematic error, is estimated to be less than 3×10^{-14}. This result is confirmed both by analysis of errors performed at the VNIIFTRI [1] and by comparison with the best foreign references of a similar type (classical cesium frequency standard using a thermal ^{133}Cs beam with a magnetic selection of atoms) and the world time unit used in the International Atomic Time System.

In the last decade, a great progress was achieved in the improvement of the accuracy of frequency standards of a new generation – atomic fountains. Due to small velocities of atoms in the fountain, many systematic frequency shifts are either absent at all or they are so small that can be estimated very accurately. Compared to a classical cesium reference, the reproducibility of the time and frequency units in the atomic fountain are better at least by an order of magnitude ($\sim 10^{-15}$), and at present the atomic fountain is the most precise time and frequency standard [3 – 7].

Although the general concept of an atomic fountain was formulated by Zacharias already in the mid-1950s [8, 9], it was implemented experimentally only after a few decades when the methods of deep laser cooling and optical trapping of atoms were developed beginning from the 1980s (see, for example, reviews [10 – 20] and references therein). The first quantitative estimates performed in pioneering papers for neutral atoms [21] and ions [22] showed that these atomic objects can be cooled down to temperatures of the order of millikelvin upon excitation by a near-resonant laser beam and the subsequent spontaneous reemission, because in the case of many events of absorption and emission of photons, atoms can be slowed down and cooled considerably and, finally, trapped by light. Hänsch and Schawlow [21] assumed that to realise this idea experimentally it is sufficient to use six laser beams directed parallel and anti-parallel to the three coordinate axes. A specific feature of laser cooling in the intersection region of the beams is that an atom performs diffuse motion during numerous absorption and emission events, i.e., as if it 'sticks' in the laser beam which is cooling the atom. As a result, the time during which the atom can leave the beam intersection region can exceed considerably the ballistic time of flight through this region. Two research groups in the USA (at Bell Labs and NBS) proposed simultaneously and independently the term 'molasses' to denote the above-mentioned specific properties of cold atoms* [23, 24].

The theoretical calculation of the minimal temperature $T_{\min}$ [29, 30] based on the balance of energies in the laser field (the Doppler limit) gives

$$k_{\mathrm{B}} T_{\min} = \frac{\hbar \Gamma}{2}. \qquad (1)$$

Here, k_{B} is the Boltzmann constant; $\hbar$ is Planck's constant; and Γ is the natural width of a resonance transition line. In the first experiments with neutral sodium atoms [31, 32], the effective temperatures ~ 70 mK were achieved, which agree with those obtained according to (1) for the Doppler limit. However, in later papers [20, 33, 34] the temperatures down

Yu.S. Domnin, G.A. Elkin, A.V. Novoselov, V.N. Baryshev, L.N. Kopylov, Yu.M. Malyshev, V.G. Pal'chikov Institute of Time and Space Metrology, Federal State Unitary Enterprise 'National Research Institute of Physicotechnical and Radiotechnical Measurements' (IMVP, FGUP VNIIFTRI), 141570 Mendeleevo, Moscow region, Russia;
e-mail: ydomnin@imvp.aspnet.ru; vitpal@mail.ru

Received 30 June 2004; revision received 5 October 2004
Kvantovaya Elektronika **34** (12) 1084 – 1095 (2004)
Translated by M.N. Sapozhnikov

* Note that this term is ambiguously treated in the Russian scientific literature as applied to a specific physical situation described above. Its literal translation is 'melassa' or 'chernaya patoka' [25]. In [26, 27], for example, the terms 'optical molasses' or simply 'optical swamp' were used, in [14] – 'viscous confinement', and one of the authors of this term, Steven Chu, considered a new form of the existence of cooled atoms as a dense, viscous liquid associated with cold: 'drawing out as molasses in January' [23]. However, critical disputes concerning this term forced Steven Chu to exclude the expression 'optical molasses' from the title of his Nobel Prize in Physics 1997 lecture, although this term was widely used in the lecture [10, 28].

to a few tens of microkelvins were achieved, which is at least an order of magnitude lower than the Doppler limit. This circumstance stimulated the development of a more realistic multilevel theory of atomic cooling, which takes into account the role of optical pumping, frequency shifts, and new mechanisms of sub-Doppler cooling (polarisation-gradient method (Sisyphean cooling), velocity-selected coherent population trapping, 'Levi statistics', optical lattices, etc.). Such a theory developed in papers [18–20, 35] considerably improved the agreement with experimental results.

The first cesium fountain on cold atoms with a working temperature of ~ 2.5 μK was developed by Andre Clairon and co-workers in 1990 [36]. In the following years, atomic fountains were also realised on sodium [37] and rubidium atoms [38–40]. The relative accuracy of cesium fountain frequency references is $\sim 1.0 \times 10^{-15}$ [5–7]. In the last two years, due to more accurate estimates of the spin-exchange collision shift, the relative reproducibility of the time and frequency standards achieved $\sim 8.0 \times 10^{-16}$ [3, 4]. Apart from very important applications as the primary time and frequency standards, the atomic fountains are successfully used in a number of fundamental studies such as the verification of the Dirac theory about the possible variations of fundamental physical constants in time [3, 4], the precision measurements of the Rydberg constant [41], the development of the atomic mass standard [10], the tests of the general theory of relativity and the string theory [42, 43], etc.

It seems that the only alternative to the use of atomic fountains for precise measurements of time and frequency is optical standards on cold atoms and ions (see, for example, [44–47]). An advantage of optical standards is a higher frequency of the so-called clock transitions (~ 100 THz and higher), which makes the achievement of a higher relative frequency stability realistic (approximately by a factor of 10^5). On the other hand, the use of the method of 'cancelled light shift' in optical standards on neutral Sr and Yb atoms opens up the possibility of improving the accuracy to $\sim 10^{-17}$ [48–51]. However, these possibilities cannot be now realised due to the extreme complexity of the experiment, and at present the relative accuracy of the best optical frequency standards does not exceed $\sim 1.0 \times 10^{-14}$ [45].

The development of a cesium frequency reference on cold atoms was initiated at the VNIIFTRI in 1999 [52, 53]. In this paper, we report the main results of the development of a cesium atomic fountain. We describe the mechanical constructions of the fountain, laser system, and microwave-field synthesiser, methods for laser stabilisation, and analyse in detail the results of the measurements. The method of adiabatic inversion of atomic states is considered in Appendix.

2. Mechanical construction of the cesium fountain

Figure 1 shows the scheme of the atomic cesium fountain developed at the VNIIFTRI. The vacuum part of the construction consists of five sections coupled with each other by flange sleeves with copper vacuum seals. The lower section, including two magnetic-ion pumps with a total pumping rate of 4 L s^{-1}, a mass spectrometer, a getter pump, and a vacuum valve, is made of a stainless steel. The other four sections [the detection region, the magneto-optical trap (MOT), the cavity region, and the free-flight or drift region] are made of titanium. The first results were obtained for the case when the detection region was located under the MOT. These two sections are mutually replaceable. The vacuum part of the device has eleven fused silica windows for injecting cooling and detecting laser beams as well as probe microwave radiation. The windows are soldered with lead to the inner surface of titanium cylinder rings, which in turn are welded to titanium vacuum flanges. The windows have AR coatings on their outer surfaces. The setup was annealed at 250 °C for 200 h during vacuum pumping. The residual pressure (5×10^{-7} Pa) was mainly determined by the partial pressure of molecular hydrogen.

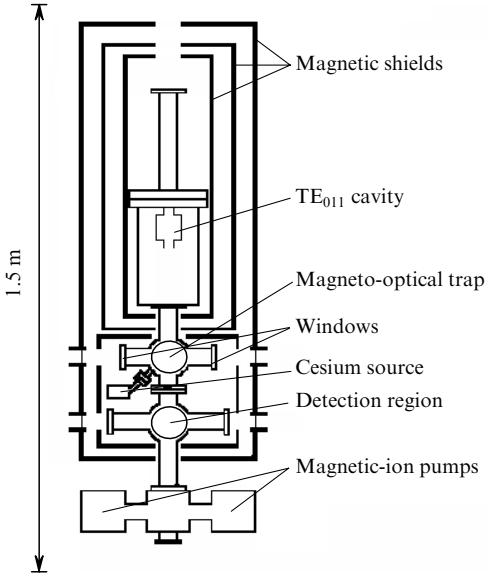

Figure 1. Scheme of the atomic cesium fountain.

A copper cylindrical microwave cavity is tuned to the TE_{011} mode. Coupling with an external signal is performed with the help of a symmetric waveguide joint through two diametrically opposite slits in the cavity walls. The Q factor of the unloaded cavity is 20 000, while that of the loaded cavity (for the chosen coupling strength) is 3000. Cut-off waveguides in the form of copper tubes of length 60 mm and diameter 11 mm are soldered to flight holes at the cavity axis to eliminate the leak of microwave radiation to the drift region. The cavity is rigidly fastened to the upper lid of the cavity section. Below, this section has a free room where we plan to place the second selecting cavity.

To separate the states of atoms with different projections of the momentum on the quantisation axis, we use the so-called C field representing a homogeneous magnetic field with the strength at which resonances at the transitions $\Delta F = \pm 1$, $\Delta m = 0$ ($F = 3$, 4 is the total momentum of a cesium atom in the ground state) are separated by a few kilohertz. The C field was produced with the help of two bias windings, one of which formed a homogeneous axial magnetic field in the upper drift region of the setup, while another produced a magnetic field in the regions of the optical trap and optical detection.

To obtain a highly homogeneous C field, the flight region of the atomic fountain, which includes the microwave

cavity and the drift region, should be shielded from external fields with a high magnetic shielding coefficient. Similarly to the bias-winding system, the magnetic-shielding system also consists of two sections: the upper and lower ones. The most important (upper) section screens the microwave cavity and the drift region. It contains a three-layer magnetic shield. The lower section, consisting of a two-layer shield and two cylinders with holes for the injection of laser radiation, shields the optical trap and the region of optical detection of atoms that have interacted in the microwave cavity. All cylindrical shields and the end lids to each of them are made of Permalloy with the magnetic penetrability about 50 000. The projected shielding efficiency, depending on the geometrical size of shields and their mutual arrangement, is 2×10^5 and 2.5×10^3 for the transverse and longitudinal coefficients of magnetic shielding, respectively.

To control accurately the effect of black-body radiation in the flight region of the fountain, heater elements of a thermostatic system are placed between the two inner layers of magnetic shields.

The rigidity of the construction is provided by four vertical bearing rods and five horizontal square plates put on these rods. The plates are also used as optical tables on which the required optical elements are mounted (Fig. 2).

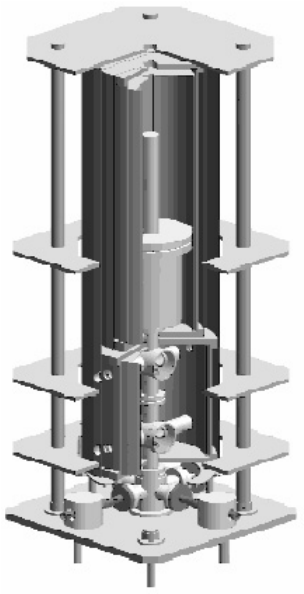

Figure 2. Construction of the mechanical part of the atomic fountain.

3. Estimates of the inhomogeneity of the C field and shielding efficiency

One of the most important corrections in the cesium fountain frequency standard (along with corrections related to black-body radiation and collisions of atoms in the flight region) is the correction for the frequency shift of the unperturbed transition (9.192631770 GHz) caused by the inhomogeneity of the static C field removing the degeneracy of the hyperfine-structure levels in the ground state of the cesium atom. This shift is determined by the known expression

$$\Delta\gamma = 427.45 \times 10^8 \langle B \rangle^2. \quad (2)$$

Hereafter, $\Delta\gamma$ is expressed in hertz and magnetic induction B in tesla. For example, for $\langle B^2 \rangle = (0.2\ \mu\text{T})^2$, the shift is $\Delta\gamma = 1.7$ mHz (or 1.9×10^{-13} in relative units). The error of measuring this shift is

$$\delta(\Delta\gamma) = 427.45 \times 10^8 \sigma^2, \quad (3)$$

where σ is the magnetic field inhomogeneity. If this inhomogeneity is 1 % of the C field strength, i.e., is 2 nT, then the relative error is $\sim 2 \times 10^{-17}$.

After assembling the system of magnetic shielding, the system producing the C field, and the system for thermostatic control, by using compensating coils for expanding the region of a highly homogeneous static field, we studied the degree of shielding of external magnetic fields (mainly the Earth field) and homogeneity of the C field, whose working strength was taken to be 6.47 mOe (or 0.647 μT for induction). In this case, the absolute frequency shift is 17.9 mHz and the relative shift is 1.95×10^{-12}.

To measure such weak magnetic fields and their variations, we used a ferroprobe representing a Permalloy core with two windings, one of which produces an alternate magnetic flux and another is used for measurements. When a sinusoidal current (in our case, with a frequency of 1 kHz) flows through the exciting winding, the magnetic state of the core changes along the dynamic hysteresis loop. In this case, an emf is induced in the measuring winding, which contains higher odd harmonics along with the fundamental frequency. When the probe is placed into a static magnetic field, which is directed, as the alternating field, along the core axis, the magnetic state of the core will change according to an asymmetric law. In this case, along with odd harmonics, even harmonics will appear in the emf signal, mainly the second harmonic, whose amplitude is proportional to the magnetic field strength. The magnetic field strength is measured from this emf.

Figure 3 shows the dependence of the magnetic field strength (C field) on the ferroprobe position on the central axis of the setup. The measurement of the magnetic field strength in the flight region of length 50 cm, including the region of interaction of atoms with microwave radiation and the free-drift region, gave the following results: the square root of the root-mean-square deviation from the mean magnetic field strength was 2.5×10^{-2} mOe for the mean field equal to 6.47 mOe or, in other words, the magnetic-field inhomogeneity was $\sigma = 2.5 \times 10^{-9}$ T. By substituting σ into (3), we obtain the relative error of measuring the frequency shift of the unperturbed transition

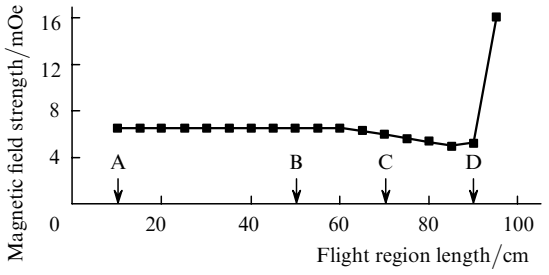

Figure 3. Dependence of the C field strength on the position of a ferroprobe on the central axis of the setup. Points A, B, C, and D indicate the positions of the upper window, microwave cavity, magneto-optical trap, and the detection region, respectively.

of the cesium atom caused by the magnetic-field inhomogeneity equal to $\delta(\Delta\gamma/\gamma) = 2.9 \times 10^{-17}$, which is acceptable for achieving the accuracy of the standard equal to 10^{-15}.

4. Laser system for cooling and detecting cesium atoms

Figure 4 shows the laser system for cooling, launching up, and detecting cesium atoms, which consists of four diode lasers. The reference and pump lasers are stabilised by an external cavity with a diffraction grating in the Littrow configuration. The two other lasers are stabilised by the injected radiation from the reference laser.

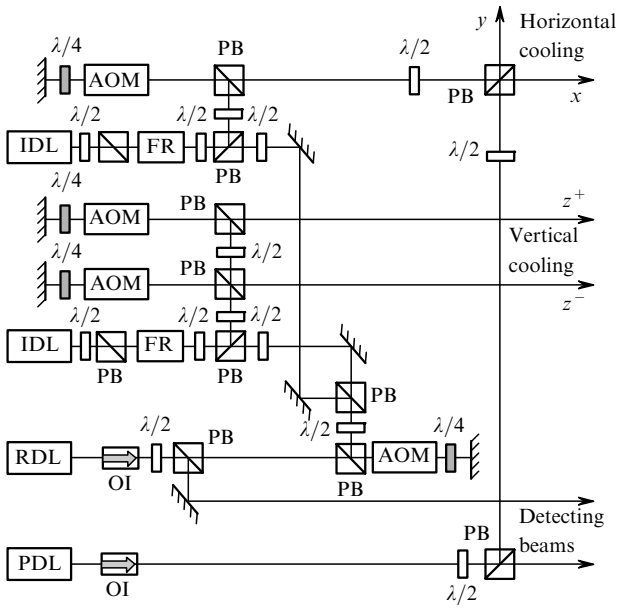

Figure 4. Simplified scheme of the laser system for cooling, launching up, and detection of atoms: RDL: reference diode laser with the external cavity; PDL: pump diode laser with the external cavity; IDL: injection diode laser; AOM: acousto-optic modulator; OI: optical isolator; PB: polarisation beamsplitter; FR: Faraday rotator; $\lambda/2$ and $\lambda/4$: half- and quarter-wave plates.

The method of automatic frequency control (AFC) of the master oscillator and pump laser we use is similar to that described in [54], except the modulation frequency of the injection current of the diode laser, which is 10 kHz in our case (80 kHz in [54]). The reference laser is tuned by the inverted saturation absorption signal, which corresponds to the cyclic $F = 4 \leftrightarrow F' = 5$ transition corresponding to the D_2 absorption line of the cesium atom. The use of inverted peaks in the AFC system simplifies its operation and improves the locking reliability.

The frequency of the pump laser is locked to the $F = 3 \leftrightarrow F' = 4$ transition. A part of its radiation is used directly at the stage of detection of atoms that have interacted in the microwave cavity, while another part, shifted in frequency by 200 MHz to the $F = 3 - F' = 3$ transition after a double passage through an acousto-optic modulator (not shown in Fig. 4), is directed to the MOT to pump atoms, which left the cooling process due to spontaneous relaxation, to the $F = 3$ level.

The radiation from the reference laser is injected into two 150-mW diode lasers. The radiation from one of them forms, in turn, four horizontal cooling beams, while the radiation from another laser forms a pair of counter-propagating vertical beams. A part of radiation from the reference laser is used to detect atoms. Polarisation-maintaining fibres (not shown in Fig. 4) are used for spatial filtration of optical beams and for delivering each of them from the optical table to the plates at which the setup is based. One of the beams is split into four cooling horizontal beams at the fibre output directly on the plate. The efficiency of radiation entering into a fibre is about 50 %.

Approximately 5 % of fluorescence photons emitted by atoms propagating in the field of a transverse standing wave is collected at the detecting photodiode. The time-integrated photodetector signal is proportional to the number of atoms in the $F = 4$ state. The linewidth of the diode laser with an external cavity (ECDL) is typically a few megahertz and is mainly limited by mechanical and acoustic vibrations of the cavity. When the laser is tuned to the optical transition frequency with the natural frequency of 5 MHz, the frequency noise caused by mechanical and acoustic external perturbations and also introduced during a direct frequency modulation of the injection current of the laser diode is inevitably transformed to the amplitude noise of the detected signal. Therefore, the improvement of frequency-noise characteristics of a semiconductor laser is an important problem.

Such frequency fluctuations can be eliminated by using a rapid negative feedback in the laser-diode injection current, which allows the stabilisation of the ECDL frequency without direct modulation of the injection current. For that purpose, the commonly acquitted Pound – Drever FM sideband technique [55, 56] with an electro-optical modulator (EOM) as an external phase modulator is usually used. It was found that an acousto-optic modulator (AOM) operating in the regime of Raman – Nath diffraction and transforming the input radiation of a single-mode diode laser to the frequency-modulated optical spectrum can be used as an external phase modulator in the method of frequency tuning by the FM side components [57]. Due to the availability and a lower cost of AOMs compared to EOMs, we propose to use the Pound – Drever method with a negative feedback in the injection current to achieve a broadband suppression of the frequency noise, narrowing of the emission spectrum, and a stable frequency tuning of ERLDs to the sub-Doppler resonances of the D_2 absorption line of the cesium atom.

The laser system is controlled by a microprocessor control system (MCS). Radiation from the reference ECDL stabilised by the saturated absorption method in cesium vapours is incident, before injection, on the AOM, which lowers its frequency by 140 – 200 MHz. The AOM provides the simultaneous frequency shift of all cooling laser beams, by changing their detuning with respect to the $F = 4 - F' = 5$ transition frequency from zero to −60 MHz. The control signal is fed to the AOM at the frequency 70 – 100 MHz from a tunable oscillator controlled by the output voltage from the MCS. In addition, the signal amplitude is corrected to obtain a sufficiently uniform transformation coefficient of the AOM over the entire frequency range. A nonlinear analogue circuit is used to transform the control signal of the AOM frequency to the correction signal modulating a high-frequency output signal of the tunable oscillator.

The output radiation of the AOM is incident on two injected lasers, and radiation from these lasers is incident on three AOMs, which increase the frequency of three formed beams used for horizontal and vertical cooling. These AOMs control the power of the beams and provide the same frequency shift Δf of the ascending and descending vertical beams at the stage of launching up of atoms. Signals at frequencies 70 MHz, 70 MHz + $\Delta f/2$, and 70 MHz – $\Delta f/2$ are fed to AOMs from the systems of formation of precision signals, each of them containing generators of frequencies 50, 70, and 90 MHz locked to the reference frequency 5 MHz by the phase control circuit. Signals at 50 and 90 MHz are mixed with the signal at the frequency 20 MHz + $\Delta f/2$, by forming signals at 70 MHz + $\Delta f/2$ and 70 MHz – $\Delta f/2$. The 70-MHz signal is used directly as the control signal for the AOM forming horizontal beams. The 20 MHz + $\Delta f/2$ signal is obtained by doubling the 10 MHz + $\Delta f/4$ signal fed from the MCS. The power of the output signals is modulated by low-frequency MCS signals.

The MCS is used for controlling the laser system, processing the detection results, and fine tuning of the microwave probe signal frequency equal to 9.192631770 GHz. The system has a two-channel analog-to-digital converter (ADC) for digitising signals from two photodetectors and four digital-to-analog converters (DACs) to control the radiation frequency and power of the horizontal, ascending, and descending beams. It also contains a system for a direct digital synthesis generating a signal at 10 MHz + $\Delta f/4$ for the frequency shift of vertical beams and sixteen transistor–transistor-logic (TTL)-compatible outputs of control signals used to switch on–switch out the pump laser, to fed the synchronisation signal to an oscilloscope, etc. We used a 16-bit sigma-delta ADC with the 10-kHz digitising rate.

5. System for the frequency stabilisation of the reference and pump lasers

The laser cooling system contains two lasers stabilised by the saturation absorption resonances in cesium. The reference laser is used to obtain the required frequency of injection lasers and to detect atoms in the $F = 4$ state. The second laser prevents optical pumping and provides the transfer of atoms from the $F = 3$ state to the $F = 4$ state. The main requirement to the laser stabilisation system is its reliability. The absorption line of cesium exhibits six saturated absorption peaks (three main and three crossover peaks) [58, 59]. The frequency of the reference laser is stabilised by using the inverted non-saturated absorption peak at the cyclic transition. The laser is stabilised by the $F = 4 \leftrightarrow F' = 5$ cyclic transition, which simply and efficiently eliminates false frequency locking at the remaining resonance absorption peaks in a cesium cell [59]. To produce an inverted resonance peak and stabilise the reference laser frequency, we used the scheme shown in Fig. 5.

The reference laser is tuned to the absorption line of cesium with the help of a diffraction grating forming the external cavity. Radiation reflected in the first order returns to the laser, while radiation reflected in the zero order is further used, as shown in the scheme in Fig. 5. The beam first passes through a prism, its elliptic cross section is transformed to the circular one, and then it passes through a Faraday isolator. The radiation is distributed with the help

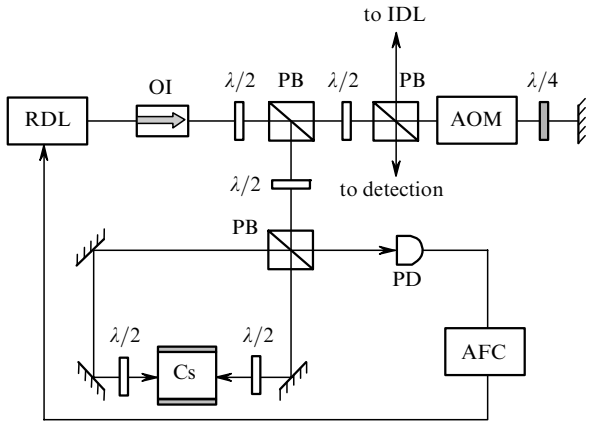

Figure 5. Scheme of using the reference diode laser: AFC: automatic frequency control; PD: photodetector; Cs: cesium cell. Other notation as in Fig. 4.

of polarisation beamsplitters and half-wave plates in the following directions: the main part of radiation (a few tens of milliwatt) is directed to the AOM and after two passages through the AOM is reflected from the polarisation beamsplitter to injection lasers. After the double passage through the AOM, the laser-beam frequency decreases by 150–210 MHz. A small part of laser radiation power (a few milliwatt) is reflected from the same polarisation beamsplitter and is directed to the detection system. Finally, ~ 1 mW of radiation is directed to the optical system to produce the inverted peak. Radiation with crossed polarisation propagates through a cesium cell placed in a magnetic shield. By using quarter-wave plates and a balance of the power of counterpropagating waves performed with the half-wave plate and polarisation beamsplitter, a strong and symmetric inverted resonance can be obtained at the $F = 4 \leftrightarrow F' = 5$ line [59]. This signal is used for laser stabilisation. Because all the other peaks are not inverted, the AFC system does not respond to them. Therefore, we have in fact one peak for frequency stabilisation and avoid false frequency locking by any other peaks.

A similar scheme can be used to stabilise the laser preventing optical pumping. However, the scheme for producing inverted peaks in this case is simpler [59]. For this laser, the inverted peak can be obtained at the $F = 3 \leftrightarrow F' = 2$ line and at the nearest crossover resonance. By using the AOM, the radiation of the laser stabilised by these two peaks can be tuned either to the $F = 2 \leftrightarrow F' = 3$ line or the $F = 3 \leftrightarrow F' = 4$ line. In both cases, such beams quite efficiently destroy optical pumping.

6. Synthesis of the interrogation 9.192631770-GHz microwave signal

New accuracy levels, which can be potentially achieved in the cesium standard, put forward new requirements to the short-term stability of the frequency of generators stabilised by the quantum resonance. In classical atomic frequency standards, the interrogation (probe) signal is synthesised by quartz oscillators with a frequency stability of $\sim(3 - 10)\times 10^{-13}$ per second. For classical cesium frequency standards having the ultimate reproducibility $\sim 10^{-14}$, such a short-term stability is quite sufficient. For hydrogen oscillators

with the long-term stability $\sim 10^{-15}$, the stability $\sim(3-10)\times 10^{-13}$ is already at the minimal admissible level because the ultimate stability is proportional to $\tau^{-1/2}$, where τ is the averaging time. For this reason, the frequency stability $\sim 10^{-15}$ in hydrogen oscillators is achieved during averaging over a day. Therefore, to measure it, about 10 days are required. It is virtually impossible to achieve the frequency stability $\sim 3\times 10^{-16}$ for atomic fountains with such quartz oscillators because this requires the processing of results at least during 100 days. Therefore, the initial short-term stability determines the achievable ultimate long-term stability, and to synthesise the interrogation signal in atomic fountain frequency standards, the oscillators having the initial stability $\sim(1-10)\times 10^{-14}$ per second are required.

At present the frequency stability per second for the best quartz oscillators is $\sim 10^{-13}$, that of the best liquid-helium-cooled oscillators with a sapphire cavity is $(2-3)\times 10^{-14}$ [60], and of the best lasers is $(1-10)\times 10^{-15}$ [61]. However, liquid-helium-cooled oscillators with a sapphire cavity are very expensive both in fabrication and operation.

We developed the scheme (Fig. 6) for synthesis of the interrogation signal at the frequency 9.192631770 GHz. In this scheme, a highly stable quartz oscillator [stability is about $(1-2)\times 10^{-13}$ per second] is phase-locked to the reference signal with the time constant ~ 30 s. A generator with the volume cavity at the frequency 1530 MHz is phase-locked to the multiplied frequency of this oscillator. To purify the frequency spectrum of this generator from the alternate component, the generator is locked by means of AFC to the frequency of a specially designed hydrogen oscillator whose power exceeds that of a conventional hydrogen oscillator approximately by a factor of 30 [62]. This allows us to hope that the short-term stability of the generator will be higher by a factor of $\sqrt{30}$ than for a conventional generator. Depending on the final stability of the hydrogen oscillator, the time constants entering the system of automatic phase control (APC) can be varied to obtain the maximum possible short-term stability of the signal at the 1530-MHz frequency.

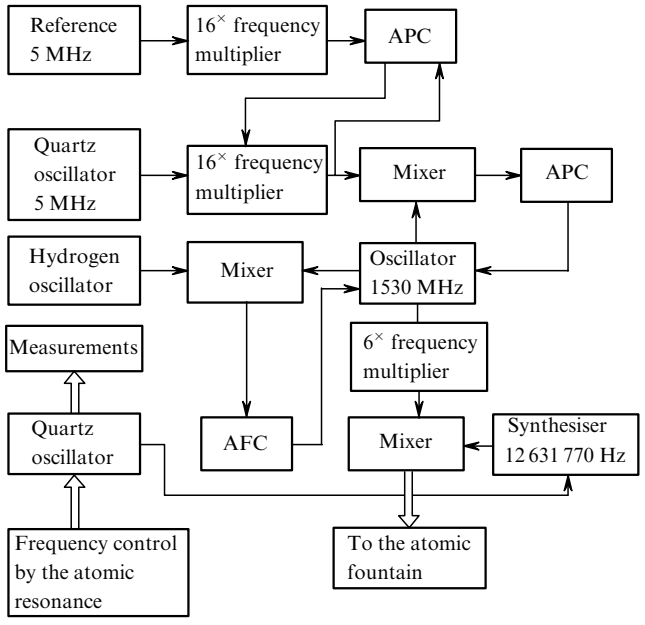

Figure 6. Scheme for synthesis of the interrogation signal frequency.

According to the scheme presented in Fig. 6, the generator frequency (1530 MHz) is increased by a factor of six and mixed with the synthesiser frequency equal to 12 631 770 Hz. The frequency of an additional highly stable quartz oscillator is used as the reference frequency of the synthesiser. This frequency is locked, in turn, by means of AFC to the maximum of the atomic resonance. By measuring the frequency of this oscillator, one can determine the frequency of the resonance.

To achieve a higher short-term stability of the interrogation signal, we developed the scheme for synthesis of its frequency (Fig. 7) based on a highly stable $He-Ne/CH_4$ laser fabricated at the P.N. Lebedev Physics Institute, RAS [63]. In this scheme, a high-power laser heterodyne is locked by means of APC to a highly stable $He-Ne/CH_4$ laser so that the modulation of the $He-Ne/CH_4$ laser is not imparted to the heterodyne [64]. The heterodyne frequency is mixed with the frequency of the diode laser used in the cooling system of the atomic fountain. The obtained signal, containing frequencies ν_{DL} and $\nu_{DL+He-Ne}$, is mixed with the signals of the comb of equidistance frequencies of a femtosecond laser. The difference frequencies ν_1 and ν_2 from photodetectors are supplied to a phase detector and then to the control of the pulse repetition rate of the femtosecond laser. The frequencies ν_1 and ν_2 are selected so that the frequencies ν_{DL} and $\nu_{DL+He-Ne}$ would be located from one side (below or above) of the nearest frequency component of the femtosecond laser. Therefore, the pulse repetition rate proves to be stabilised by the frequency of the $He-Ne/CH_4$ laser. The slave generator, which is used for synthesis of the frequency at 9192.631770 MHz, is locked, in turn, to the pulse repetition rate. The atomic-resonance signal is supplied to the control circuit of the laser heterodyne to achieve an accurate tuning to the maximum of the atomic resonance. The diode laser frequency does not affect the synthesised signal, and it can be locked to an optical transition in the cesium atom to improve the operation reliability. To do this, it is sufficient to branch off a fraction of the power of the reference laser in the cooling system of the atomic fountain.

Such a scheme for synthesis of the interrogation signal can be very efficient because all the resources in the radio-frequency and microwave ranges for obtaining the short-term stability are virtually exhausted, whereas in the optical range the short-term stability of the order of 10^{-15} per

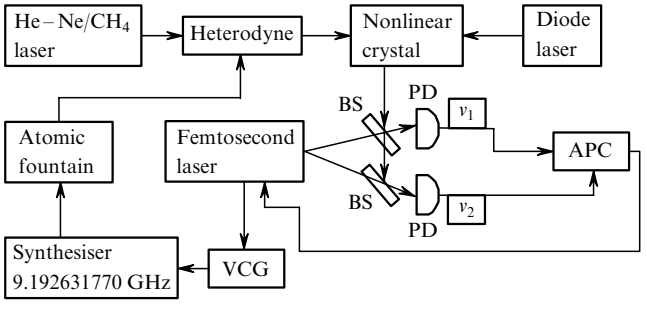

Figure 7. Scheme for synthesis of the interrogation signal frequency from the frequency of a highly stable $He-Ne/CH_4$ laser: VCG: voltage-controlled generator; BS: beamsplitter.

second can be achieved, and thus stability can be transferred to the radio-frequency range with the help of femtosecond lasers.

A specific feature of the scheme is also that the frequency of the $He-Ne/CH_4$ laser can be measured with high accuracy from the frequency of the atomic fountain. If the $He-Ne/CH_4$ laser is replaced, for example, by a CO_2/OsO_4 laser or any other IR or visible laser, whose frequency can be mixed in a nonlinear crystal with the diode laser frequency, then the frequency of this laser also can be measured with high accuracy. Therefore, the scheme presented above solves at the same time the problems of precision frequency measurements and the extension of applications of the frequency standard to the IR and visible spectral ranges.

7. Results of experimental observations

The first tests of the system were performed with atoms cooled in a magneto-optical trap. Two anti-Helmholtz coils were placed near the trap, which produced the gradient of the magnetic field strength up to 10 Oe cm^{-1}. The frequency of cooling beams with the power density ~ 2 mW cm^{-2} was detuned by a few megahertz from the frequency of the $F = 4 \leftrightarrow F' = 5$ cyclic transition. In this case, Doppler cooling of atoms was performed. The expression for the limiting temperature of Doppler cooling is presented in Introduction; for cesium, it is about 120 μK. We obtained cooled atoms, which were observed with the help of an IR camera. The maximum brightness of emission of an atomic cloud was observed when the number of confined atoms was maximal and the frequency of laser beams was detuned approximately by 3 MHz below the optical resonance frequency. When the magnetic field and laser beams were switched off, the atoms did not drop but were thrown up upward and sideways under the action of the magnetic field of Earth. When the anti-Helmholtz coils were switched off, the region of zero magnetic field displaced upward and imparted the momentum to the cold atomic cloud in the same direction. This effect was eliminated when the confinement region of atoms was shielded by means of the magnetic shield.

Further experiments were performed in the absence of the magnetic field, i.e., the atoms were confined and cooled in the so-called optical molasses (see footnote in Introduction). In this case, not only Doppler but also Sisyphean cooling was preformed [12, 65]. We used the cycle during which the atoms were first accumulated in the beam interaction region, where Doppler cooling occurred. After about 0.5 s, the frequency of cooling laser beams was linearly decreased approximately by 50 MHz and simultaneously the power of laser beams was reduced by an order of magnitude. The temperature of cold atoms is proportional to the intensity of cooling beams and is inversely proportional to the frequency detuning, provided the detuning is larger than the optical resonance width. The limiting temperature is determined by the expression $kT_r \approx 4\pi^2\hbar^2/(M\lambda^2)$, where M is the atom mass and λ is the wavelength of cooling radiation. For cesium, the limiting temperature is close to 0.1 μK.

7.1 Determination of the number of trapped atoms

In experiments on cooling and trapping atoms in the optical molasses, the sensitivity of the IR camera is no longer sufficient for determining the number of confined atoms because the density of atoms in the molasses is much lower than in the MOT. For this reason, we determined the number of trapped atoms by estimating the number of cold atoms flying past a detector located 20 cm below the trapping region.

The detected signal had the form of a distinct burst caused by the atomic cloud flying through the beam (Fig. 8). The signal appears within 0.2 s after switching off laser beams. The signal duration determined by the flying atomic cloud is about 7 ms, which corresponds to the cloud diameter 15 mm. We will estimate the number of atoms in the cloud based on the geometrical dimensions of the setup and the noise properties of the photodiode.

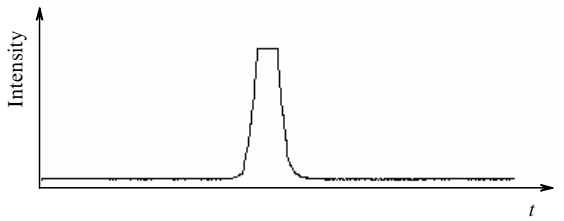

Figure 8. Free fall of the atomic cloud (signal is cut due to amplifier saturation). Here and in Figs 9, 10, 13, and 14, the sweep duration is 102.4 ms.

The distance from the output window of the setup to its centre (axis line) is 40 mm and the output window diameter is also 40 mm. With such a geometry, we can expect that radiation will be collected within a solid angle of 0.66 sr, which corresponds to the theoretical efficiency of radiation collection equal to $0.66/4\pi$, or 5.25 %.

The diameter of the detected beam is 4 mm. Because atoms fall from the height $h = 20$ cm over the detection region, they fly to the detection region for the time $t = 0.2$ s, where they acquire the velocity $v = 2$ m s^{-1} and, hence, intersect the detected beam for the time 2×10^{-3} s.

An atom scatters one photon for about 10^{-7} s, which means that an atom flying through the detection region reemits approximately 20 000 photons. In reality, this number is smaller because of losses in optical elements and due to finite dimensions of the emission region. By estimating the losses in the radiation collection system as 50 %, we obtain that 500 photons are incident on a photodetector. Their total energy is $N_{h\nu} = 1.16 \times 10^{-16}$ J. This corresponds to a power of 7.3×10^{-16} W per the 1-Hz bandwidth.

According to the certificate, the equivalent noise power of our photodiode is 4.3×10^{-15} W Hz^{-1}. This means that, to achieve the signal-to-noise ration equal to unity, we need approximately six atoms. The observed signal-to-noise ratio in the 1-Hz bandwidth was estimated to be about 200 000, which corresponds to about 10^6 atoms found in the detection region. We neglected, however, the electronic noise, which can be roughly estimated as ~ 20 dB. Therefore, a total number of atoms in the cloud can be estimated as $10^6 - 10^7$.

7.2 Throwing up of atoms and determination of their temperature

A simple drop of atoms from the confinement region does not allow us to determine the cloud temperature because we

can perform only one measurement having two unknown parameters: the initial diameter of the cloud and its temperature. However, the regime of launching up of atoms to different heights allows us to measure the initial diameter and temperature of the cloud from two measurements.

We used the following regime of launching up of atoms. The atoms first were accumulated in the optical molasses for 0.6 s. The initial detuning from the optical resonance was 8 MHz. Then, the frequency of the lower vertical beam was tuned to the frequency $\nu_3 - \Delta f$, while the frequency of the upper vertical beam was tuned to the frequency $\nu_3 + \Delta f$. Here, ν_3 is the detuning from the optical resonance frequency equal to 3 MHz and Δf is the frequency determined by the velocity that we wish to impart to the atomic cloud. To impart the velocity of 1 m s^{-1}, the frequency Δf equal to 1 MHz is required. The duration of this process is 1 ms. Then, the atomic cloud is further cooled during the flight in the intersection region of all the beams. For this purpose, their frequencies are reduced linearly by 60 MHz for 1 ms and simultaneously the power is reduced linearly down to 10 % of the initial value. Then, all the beams are switched off, and a free ballistic flight of the atomic cloud occurs. For the maximum launching up height, the time of the flight from the optical molasses to the detection region is about 0.8 s.

We performed experiments on launching atoms with different velocities both upward and downward. By launching atoms downward with a great initial velocity (for example, 3 m s^{-1}), we determined experimentally the initial diameter of the atomic cloud from its time of flight through the detection region. Because the cloud reaches the detection region virtually at once (approximately for 60 ms), no significant diffusion of the cloud can occur for such a short time. This means that we can determine the initial cloud diameter from the detection duration and the known flight velocity. According to our estimates, the typical initial diameter is 10 mm.

Figure 9 shows the signals obtained from the atomic cloud after imparting the initial velocity to it. The signal presented in Fig. 9a was obtained as follows. The cloud thrown up with the initial velocity of 3.3 m s^{-1} rises to a height of 56 cm and falls downward, flying through the detection region within 0.76 s after the instant of launching up. In a given case, the initial cloud diameter was 10 mm, the final diameter was 21 mm, and the temperature was 1.8 μK. The signal shown in Fig. 9b was obtained by launching the cloud downward at a velocity of 3 m s^{-1}. In this case, the cloud flies through the detection region within 0.06 s after the instant of launching. One can see that the signal width (i.e., the flight time) is approximately half the time in the previous case.

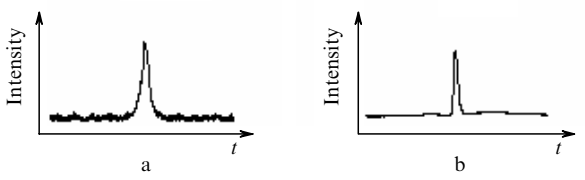

Figure 9. Fluorescence signals from the atomic cloud thrown up at the velocity 3.3 m s^{-1} (a) and thrown down at the velocity 3 m s^{-1} (b).

7.3 Determination of the cloud diameter in the apogee

When the atomic cloud is thrown up at the velocity above 3.4 m s^{-1}, it collides with the upper window of the setup. By varying the launching up velocity, we can make a part of the cloud collided with the upper window to be cut. From the response of a partially cut cloud – a step-wise change of the signal from the cloud, the so-called cut, we can determine the cloud diameter at the apogee and compare it with the calculated value. If the initial cloud diameter was close to zero, the cut of the cloud during its flight could not spread, and we would observe it in the signal. But because the initial diameter is about 10 mm, the cut spreads during the fall of the cloud due to the diffusion of atoms. The slope of the cut gives the rate of its spread and, hence, allows us to determine the temperature of the cloud. Figure 10 shows the two cuts of the atomic cloud from which we determined the cloud temperature and diameter in the apogee.

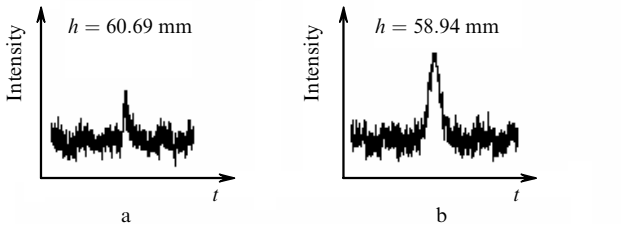

Figure 10. Cuts of the atomic cloud thrown up to different heights at the initial velocity 3.45 (a) and 3.4 m s^{-1} (b). The atomic cloud diameter in the apogee is 17.5 mm; the cloud temperature determined from the cut is ~ 5 μK.

7.4 Interchange of the detection and trapping regions

When the setup operated in the regime of an atomic spectroscope, the molasses region is located below, while the detection region is located 20 cm higher. The source of cesium atoms is placed closer to ionic pumps and much farther from the flight region, which allows one to reduce significantly both the flux of background cesium atoms in the flight region and their possible effect on the frequency shift of the atomic transition. In this case, we can no longer detect cold atoms without their launching up. However, the possibility appears to detect the atomic cloud flying upward and falling down. The detection of the falling cloud is more important because in this case the atoms are in a free flight for about 1 s. To determine the temperature and diameter of the atomic cloud, we detected the cloud by launching it up at the initial velocities from 2.3 to 3.7 m s^{-1} (with a step of 0.05 m s^{-1}). We developed the program code for data processing which allows us to determine both the temperature and diameter of the cloud from the dependence of the detection instance of atoms on their initial velocity. The program contained the initial cloud diameter equal to zero. This dependence should be approximated by a straight line, whose intersection with the abscissa gives the cloud temperature, while the slope of the straight line gives the real initial diameter. If the program uses the real initial cloud diameter, then all the points should lie on a straight line parallel to the abscissa, and the height of this straight line along the ordinate will give the cloud temperature. Figure 11 shows the results of such processing, which give

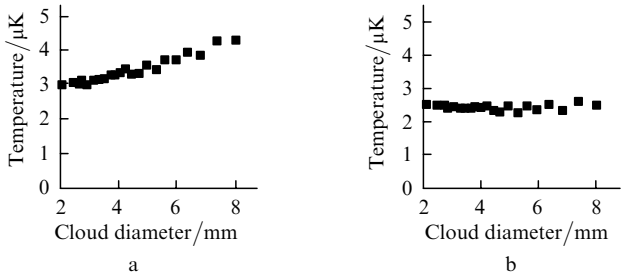

Figure 11. Dependences used for determining the atomic cloud temperature and diameter for the initial cloud diameter equal to zero (a) and 9 mm (b).

the cloud temperature about 2.5 μK and the initial cloud diameter ~ 9 mm.

7.5 Use of retroreflectors

To inject and separate horizontal beams in the setup, we used the scheme shown in Fig. 12. The cooling beam is incident on an angular polarisation beamsplitter and is split by means of a half-wave plate into two equal parts. The pump laser beam is incident on the same beamsplitter. Then, the beams are directed to the next beamspltters so that the half-wave plates in front of them balance only counterpropagating beams and has no effect on perpendicular beams (i.e., the beams propagating along the x-axis do not affect the beams propagating along the y-axis, and vice versa). In these directions, half-wave plates are located to produce the mutually perpendicular polarisation of the counterpropagating beams. To enhance the light intensity, the beams were returned to the setup by means of additional retroreflectors. In this case, they propagated in the same direction as the forward beams, but had perpendicular polarisation. This casts some doubt on the efficiency of using retroreflectors. However, the experimental results showed that the number of cooled atoms was approximately doubled when these mirrors were used.

Figure 13 shows the signals obtained when atoms were thrown up at a velocity of 3.3 m s^{-1} in the case of open and closed retroreflectors.

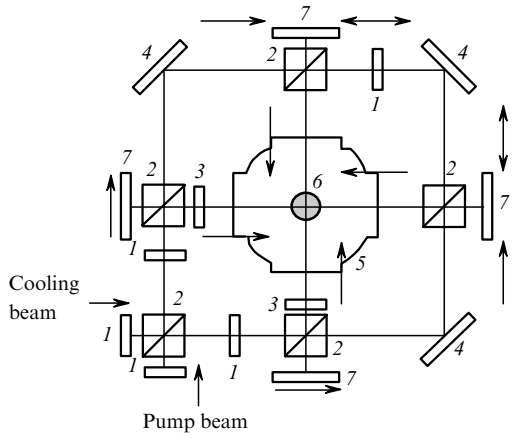

Figure 12. Scheme for directing horizontal beams: (*1*) half-wave plates; (*2*) polarisation beamsplitters; (*3*) half-wave plates for producing mutually perpendicular polarisation; (*4*) additional mirrors; (*5*) vacuum chamber; (*6*) cold atomic cloud; (*7*) retroreflectors.

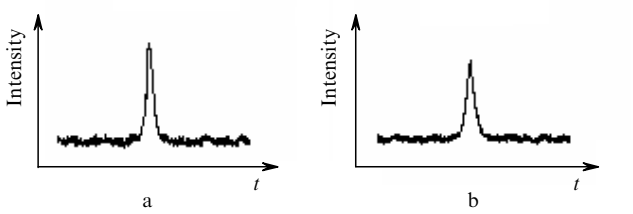

Figure 13. Signals obtained by launching up atoms to the operating height at the velocity 3.3 m s^{-1} at closed (the relative integrated signal intensity is $s = 11000$, temperature $T = 1.2$ μK) (a) and open ($s = 17500$, $T = 1.4$ μK) (b) retroreflectors.

7.6 Preliminary experiments on interaction with microwave radiation

We used only one detector in experiments on cooling and control of the motion of the atomic cloud. The detection system was tuned to the $F = 4 \leftrightarrow F' = 5$ transition because all the cooled atoms are in the $F = 4$ state. The $F = 4$ state consists of nine sublevels, so that it is virtually impossible to observe their change caused by microwave radiation by detecting atoms in this state. Even when the atoms completely transfer from the $F = 4$, $m = 0$ state to the $F = 3$, $m = 0$ state, the total number of atoms in the $F = 4$ state decreases by 11 %. At the same time, the natural fluctuations of the total number of atoms from launching up to launching up are within 10 %, so that the action of microwave radiation is comparable with natural fluctuations.

To observe the interaction of atoms with microwave radiation, we proposed to pump optically cold atoms to the $F = 3$ state. After all the atoms transfer to this state, microwave radiation excite the atoms from the $F = 3$, $m = 0$ state to the $F = 4$, $m = 0$ state. In this case, only the atoms that have interacted with microwave radiation are detected.

To perform optical pumping after additional cooling of atoms during the flight, the pump laser was switched off by 5 ms earlier than the cooling beams, the power of the beams being invariable during additional cooling to enhance the efficiency of optical pumping. The results of optical pumping are presented in Fig. 14. One can see that almost 100 % of atoms transfer to the $F = 3$ state, which is accompanied by some increase in the cloud temperature (Fig. 14b). Nevertheless, this does not prevent the observation of the interference Ramsey oscillations.

Our preliminary studies gave Ramsey oscillations with the width of the resonance of ~ 1 Hz. The width of the Rabi pedestal was 60 Hz. The strength of the C field in the flight region of the atomic fountain was determined from the $F = 3$, $m = 1 \leftrightarrow F = 4$, $m = 1$ transitions.

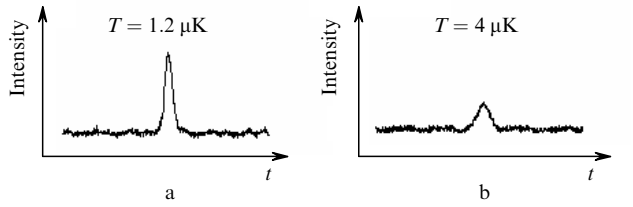

Figure 14. Signal obtained from the atomic cloud thrown up to the operating height (a) and the signal obtained under the same conditions, but in the case of a constant power of the beams, at which complete transfer to the $F = 3$ state occurs (b).

8. Conclusions

We have performed experimental studies with the aim of developing an atomic fountain – a quantum frequency standard on cold cesium atoms. We have developed the laser system for cooling, launching up, and detection of atoms, which is controlled by a microprocessor providing the automated computer processing of the detection results and control of the frequency of the probe microwave signal. The reference and pump lasers were stabilised by saturated absorption resonances in a shielded cesium cell. A high short-term stability of the frequency of the interrogation microwave signal was achieved by using two original schemes for the frequency synthesis, which employ a specially developed high-power hydrogen oscillator, a highly stable $He-Ne/CH_4$ laser, and a mode-locked femtosecond laser.

The first preliminary results are reported on the observation of Ramsey oscillations in the atomic fountain with the width of the central resonance ~ 1 Hz upon cooling cesium atoms down to ~ 2 μK.

We intend to use the acquired experience and methods used in the paper for the development of a fountain frequency reference with the non-excluded systematic uncertainty $\sim 10^{-15}$, which will be used in the State primary time and frequency standard of the Russian Federation.

Acknowledgements. The authors thank Andre Clairon (Paris Observatory, France), Andreas Bauch, and Stephen Weyers (Physikalisch-Technische Bundesanstalt) for discussions, consultations, and interest in this study. This work was partially supported by the Ministry of Science and Technologies of the Russian Federation [Contract No. GNTD/GK-021(00)] and the extra-budget foundation of the State Standard of the Russian Federation.

Appendix

Theoretical calculation of the adiabatic inversion of atomic states in cesium

As mentioned in Introduction, the spin-exchange collision shift is one of the sources of a systematic uncertainty in measurements of the clock-transition frequency in an atomic fountain. The measurement errors of the collision shift are, as a rule, rather large ($\sim 10\,\%$, see [66, 67]), while the corresponding theoretical estimates [68] are quite complex, nontrivial, and also are not sufficiently accurate and reliable. In the methods for collision shift measuring (irrespective of the general approach), it is necessary to know the population density of atomic states determining the clock transition (more exactly, the population ratio). The authors of papers [3, 69] proposed and realised the method of adiabatic population inversion of atomic states upon excitation of atoms by a Blackman pulse in a microwave cavity. In this method, the population probabilities of the states are exactly equal to 1/2 and 1 at certain instants $t = T/2$ and $t = T$ (where T is the pulse propagation time). Not analysing in detail the advantages and limitations of this method, we note only that this method is rather simple and provides the measurement of the spin-exchange collision shift with the error $\sim 1\,\%$ [3, 69]. We intend to use the method of adiabatic inversion in the cesium fountain developed at the VNIIFTRI. In this connection, we calculated by this method the population probabilities for the $|F = 4, m = 0\rangle \rightarrow |F = 3, m = 0\rangle$ transition for six microwave pulses.

In the general case, the electromagnetic field was described by the expression

$$E = E_0 f(t) \cos \omega t, \tag{A1}$$

where E_0 is the field amplitude and the function $f(t)$ describes the time dependence of the pulse shape and satisfies the normalisation condition

$$\int_{-\infty}^{\infty} f(t) \mathrm{d}t = 1. \tag{A2}$$

In the rotating wave approximation [26], the Bloch equations for a two-level system are written in the form

$$\begin{aligned} \frac{\partial C_\alpha}{\partial t} &= -\mathrm{i}Bf(t) \exp(\mathrm{i}at) C_\beta, \\ \frac{\partial C_\beta}{\partial t} &= -\mathrm{i}Bf(t) \exp(-\mathrm{i}at) C_\alpha. \end{aligned} \tag{A3}$$

Here, C_α and C_β are the probability amplitudes for a two-level system; $B = -D_\mu E_0 T/2\hbar$ is the dimensionless constant; D_μ is the dipole matrix element; and $a = (\omega - \omega_0)T$ is the frequency detuning. The results of numerical calculations are presented in Fig. 15 and Table 1.

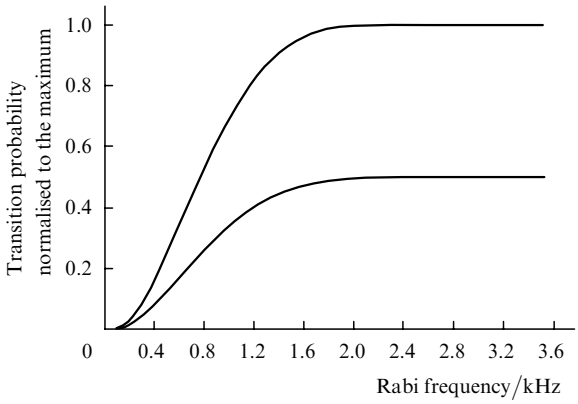

Figure 15. Transition probability for the Blackman pulse of duration 5 ms for a frequency detuning of 5 kHz.

The transition probabilities were calculated by determining the frequency detuning from the solution of the differential equation

$$\frac{\partial a}{\partial t} = \Omega^2(t), \tag{A4}$$

where $\Omega/2\pi$ is the Rabi frequency. One can see from the curves in Fig. 15 and Table 1 that the probabilities $W1$ and $W2$ are close to exact values 1/2 and 1 and rather weakly depend on the pulse shape in the microwave cavity. For the Blackman pulse (Fig. 15), the results of our calculations well agree with the results of independent calculations and experiments presented in [3, 69].

Table 1. Probabilities of the $|F=4, m=0\rangle \rightarrow |F=3, m=0\rangle$ transition for $t=T/2$ ($W1$) and $t=T$ ($W2$) for $T=4$ ms and the maximum frequency detuning 4 kHz.

Pulse shape	Formula	$W1$	$W2$
Rosen – Zener	$f(t)=\frac{1}{2}\operatorname{sech}\frac{\pi t}{2}$	0.5004	1.0009
Quadratic Rosen – Zener	$f(t)=\frac{\pi}{4}\operatorname{sech}^2\frac{\pi t}{2}$	0.5001	1.0000
Lorentzian	$f(t)=\left(\frac{2}{\pi}\right)^{1/2}\frac{1}{1+t^2}$	0.5008	1.001
Quadratic Lorentzian	$f(t)=\frac{2}{\pi(1+t^2)^2}$	0.5005	1.001
Gaussian	$f(t)=\frac{1}{\sqrt{\pi}}\exp\left(-t^2\right)$	0.5004	1.0008

References

1. Gaigerov B.A., Elkin G.A., Zagirova E.G., Kostromin V.P., Koshelyavskii N.B., Pushkin S.B. *Kosmonavt. Raketostr.*, **29**, 31 (2002).
2. Baryshev V.N., Elkin G.A., Yakovlev Yu.N. *Izmereniya v oblasti vremeni i chastoty* (Time and Frequency Measurements) (Moscow: Izd. VNIIFTRI, 1990).
3. Pereira Dos Santos F., Marion H., Abgrall M., Zhang S., Sortais Y., Bize S., Maksimovic I., Calonico D., Grunert J., Mandache C., Vian C., Rosenbuch P., Lemonde P., Santarelli G., Clairon A. *Proc. Frequency Control Symp. and PDA Exhibition Jointly with the XVII Europ. Frequency and Time Forum* (Tampa, USA, 2003) pp 55 – 67.
4. Marion H., Pereira Dos Santos F., Abgrall M., Zhang S., Sortais Y., Bize S., Maksimovic I., Calonico D., Grunert J., Mandache C., Lemonde P., Santarelli G., Laurent P., Clairon A., Salomon C. *Phys. Rev. Lett.*, **90**, 150801 (2003). doi
5. Weyers S., Hubner U., Schroder R., Tamm Chr., Bauch A. *Metrologia*, **38**, 343 (2001). doi
6. Jefferts S.R., Meekhof D.M., Heavner T.P., Parker T.E. *Metrologia*, **39**, 321 (2002). doi
7. Salomon C., Sortais Y., Bize S., Abgrall M., Zhang S., Nicolas C., Mandache C., Lemonde P., Laurent P., Santarelli G., Clairon A., Dimarco N., Petit P., Mann A., Luiten A., Chang S. *Proc. XVII Int. Conf. At. Phys.* (Melville, New York, 2001) p. 23.
8. Zacharias J.R. *Phys. Rev.*, **94**, 751 (1954).
9. Ramsey N.F. *Molecular Beams* (Oxford: Clarendon Press, 1956).
10. Chu S. *Usp. Fiz. Nauk*, **169**, 274 (1999).
11. Phillips W.D. *Usp. Fiz. Nauk*, **169**, 305 (1999).
12. Cohen-Tannoudji C. Usp. *Fiz. Nauk*, **169**, 292 (1999).
13. Letokhov V.S., Chebotaev V.P. *Nelineinaya lazernaya spektroskopiya sverkhvysokogo razresheniya* (Nonlinear Ultrahigh-resolution Laser Spectroscopy) (Moscow: Nauka, 1990).
14. Kazantsev A.P., Surdutovich G.I., Yakovlev V.P. *Mekhanicheskoe deistvie sveta na atomy* (Mechanical Action of Light on Atoms) (Moscow: Nauka, 1991).
15. Harold J. Netcalf, Peter van der Straten. *Laser Cooling and Trapping* (Berlin: Springer – Verlag, 1999).
16. Chang S., Minogin V. *Phys. Rep.*, **365**, 65 (2002). doi
17. Balykin V.I., Minogin V.G., Letokhov V.S. *Rep. Prog. Phys.*, **63**, 1429 (2000). doi
18. Dalibard J., Cohen-Tannoudji C. *J. Opt. Soc. Am. B.*, **6**, 2023 (1989).
19. Lett P.D., Phillips W.D., Rolston S.L., Tanner C.E., Watts R.N., Westbrook C.I. *J. Opt. Soc. Am. B.*, **6**, 2084 (1989).
20. Ungar P.J., Weiss D.S., Riis E., Chu S. *J. Opt. Soc. Am. B.*, **6**, 2058 (1989).
21. Hansch T., Schawlow A.L. *Opt. Commun.*, **13**, 68 (1975). doi
22. Wineland D., Dehmelt H. *Bull. Am. Phys. Soc.*, **20**, 637 (1975).
23. Chu S., Hollberg L., Bjorkholm J., Cable A., Ashkin A. *Phys. Rev. Lett.*, **55**, 48 (1985). doi
24. Phillips W.D., Prodan J., Metcalf H. *J. Opt. Soc. Am. B.*, **2**, 1751 (1985).
25. Apresyan Yu.D., Gal'perin I.P., Ginzburg R.S., Ershova I.F., Kalantarova L.L., Mendishova E.M., Petrova F.V., Fel'dman M.E. *Bol'shoi anglo-russkii slovar'* (English-Russian Dictionary) (Moscow: Russkii Yazyk, 1987), Vol. 1.
26. Mandel L., Wolf E. *Optical Coherence and Quantum Optics* (Cambridge, 1995).
27. Oduan K., Gino B. *Izmerenie vremeni. Osnovy GPS* (Time measurements. The fundamentals of GPS) (Moscow: Tekhnosfera, 2002).
28. Chu S. *The Nobel Foundation. Nobel Prize in Physics 1997* (The Royal Swedish Academy of Science, 1998).
29. Letokhov V.S., Minogin V.G., Pavlik B.D. *Zh. Eksp. Teor. Fiz.*, **72**, 1328 (1977).
30. Wineland D., Itano W. *Phys. Rev. A*, **20**, 1521 (1979). doi
31. Phillips W.D., Metcalf H. *Phys. Rev. Lett.*, **48**, 596 (1982). doi
32. Prodan J., Phillips W.D., Metcalf H. *Phys. Rev. Lett.*, **49**, 1149 (1982). doi
33. Lett P., Watts R., Westbrook C., Phillips W.D., Could P., Metcalf H. *Phys. Rev. Lett.*, **61**, 169 (1988). doi
34. Chu S., Preutiss M.G., Cable A.E., Bjorkholm J.E. *Laser Spectroscopy* (New York: Springer – Verlag, 1987) Vol. 8, p. 78.
35. Cohen-Tannoudji C., Phillips W.D. *Phys. Today*, **43**, 33 (1990).
36. Salomon C., Dalibard J., Phillips W.D., Clairon A., Guellati S. *Europ. Lett.*, **12**, 683 (1990).
37. Kasevich M.A., Riis E., Chu S., DeVoe R.G. *Phys. Rev. Lett.*, **63**, 612 (1989). doi
38. Kokkelmans S.J.J.M.F., Verhaar B.J., Gibble K., Heinzen D.J. *Phys. Rev. A*, **56**, 4389 (1997). doi
39. Fertig C., Gibble K. *Phys. Rev. Lett.*, **85**, 1622 (2000). doi
40. Bize S., Sortais Y., Santos M.S., Mandache C., Clairon A., Salomon C. *Europ. Lett.*, **45**, 558 (1999). doi
41. Niering M., Holswarth R., Reichert J., Pokasov P., Udem T., Weitz M., Hansch T., Lemonde P., Santarelli G., Abgrall M., Laurent P., Salomon C., Clairon A. *Phys. Rev. Lett.*, **84**, 5496 (2000). doi
42. Damour T., Polyakov A. *Nucl. Phys. B*, **423**, 532 (1994). doi
43. Damour T., Piazza F., Veneziano G. *Phys. Rev. Lett.*, **89**, 081601 (2002). doi
44. Baklanov E.V., Pokasov P.V. *Kvantovaya Elektron.*, **33**, 383 (2003) [*Quantum Electron.*, **33**, 383 (2003)]. doi
45. Lea S.N., Margolis H.S., Huang G., Rowley W.R.C., Handerson D., Barwood G.P., Klein H.A., Webster S.A., Plythe P., Gill P. *Proc. VI Symp. Frequency Standards and Metrology* (World Scientific, 2002) p. 144.
46. Curtis E.A., Oates C.W., Diddams S.A., Udem Th., Hollberg L. *Proc. VI Symp. on Frequency Standards and Metrology* (World Scientific, 2002) p. 331.
47. Wilpers G., Binnewies T., Degenhardt C., Helmcke J., Riehle F. *Phys. Rev. Lett.*, **89**, 230801 (2002). doi
48. Pal'chikov V.G., Ovsiannikov V.D. *Proc. Frequency Control Symp. and PDA Exhibition Jointly with the XVII Europ. Frequency and Time Forum* (Tampa, Florida USA, 2003) p. 142.
49. Pal'chikov V.G., Ovsiannikov V.D. *Kvantovaya Elektron.*, **34**, 412 (2004) [*Quantum Electron.*, **34**, 412 (2004)]. doi
50. Katori H., Takamoto M., Pal'chikov V.G., Ovsiannikov V.D. *Phys. Rev. Lett.*, **91**, 173005 (2003). doi
51. Pal'chikov V.G., Ovsiannikov V.D. *Proc. SPIE Int. Soc. Opt. Eng.*, **5478**, 219 (2004).
52. Domnin Yu.S., Elkin G.A., Novoselov A.V., Kopylov L.N., Barychev V.N., Pal'chikov V.G. *Can. J. Phys.*, **80**, 1321 (2002). doi
53. Domnin Yu.S., Elkin G.A., Novoselov A.V., Kopylov L.N., Barychev V.N., Pal'chikov V.G. *Proc. Frequency Control Symposium and PDA Exhibition Jointly with the XVII Europ. Frequency and Time Forum* (Tampa, Florida USA, 2003) p. 127.
54. Rovera G.D., Santarelli G., Clairon A. *Rev. Sci. Instr.*, **65**, 1502 (1994). doi
55. Drever R., Hall J., Kovalski F., Hough J., Ford G., Munley A., Ward H. *Appl. Phys. B*, **31**, 97 (1983). doi
56. Bjorklund G., Levenson M., Lenth W., Ortiz C. *Appl. Phys. B*, **32**, 145 (1983). doi
57. Baruchev V. *Proc. SPIE Int. Soc. Opt. Eng.*, **5480**, 20 (2004).

58. Akul'shin A.M., Velichanskii V.L., Gamidov R.G., Izmailov A.Ch., Popovichev V.V., Sautenkov V.A. *Zh. Eksp. Teor. Fiz.*, **99**, 107 (1991).
59. Domnin Yu.S., Tatarenkov V.M., Novoselov A.V., Pal'chikov V.G. *Proc. VI Symp. Frequency Standards and Metrology* (World Scientific, 2002) p. 600.
60. Santarelli G., Laurent P., Lemonde P., Clairon A., Mann A.G., Chang S., Luiten A.V., Salomon C. *Phys. Rev. Lett.*, **82**, 4619 (1999).
61. Hall J.L., Ma L.S., Taubman M., Tiemann B., Hong F.L., Pfister O., Ye J. *IEEE Trans. Instr. Meas.*, **48**, 583 (1999).
62. Boyko A., Yolkin G., Gestkova N., Kurnikov G., Paramzin V. P*roc. XV Europ. Frequency and Time Forum* (Neuchatel, Switzerland, 2001) p. 406.
63. Gubin M., Kovalchuk E., Petrunkin E., Shelkovnikov A., Tyurikov D., Gamidov R., Erdogan C., Sahin E., Felder R., Gill P., Lea S.N., Kramer G., Lipphardt B. *Proc. VI Symp. Frequency Standards and Metrology* (World Scientific, 2002) p. 453.
64. Domnin Yu.S. *Izmer. Tekhn.*, (6), 236 (1986).
65. Jersblad J., Ellmaun H., Kartberg A. *Phys. Rev. A*, **62**, 51401 (2000).
66. Gibble K., Chu S. *Phys. Rev. Lett.*, **70**, 1771 (1993).
67. Leo J.L., Julienne P.S., Mies F.H., Williams C.J. *Phys. Rev. Lett.*, **86**, 3743 (2001).
68. Bouchoule I., Morinaga M., Salomon C., Petrov D. *Phys. Rev. A*, **65**, 0033402 (2002).
69. Pereira Dos Santos F., Marion H., Bize S., Sortais Y., Clairon A., Salomon C. *Phys. Rev. Lett.*, **89**, 233004 (2002).